

RESEARCH ARTICLE | APRIL 07 2025

Probabilistic flux limiters ^{EP}

Nga Nguyen-Fotiadis ^{ID}; Robert Chiodi ^{ID}; Michael McKerns ^{ID}; Daniel Livescu ^{ID}; Andrew Sornborger [✉] ^{ID}



Physics of Fluids 37, 046112 (2025)

<https://doi.org/10.1063/5.0254069>



Articles You May Be Interested In

The implementation of fault tree analysis approaches in nuclear power plant probabilistic safety assessment

AIP Conf. Proc. (December 2019)

Machine learning changes the rules for flux limiters

Physics of Fluids (August 2022)

Probabilistic deep learning of turbulent premixed combustion

AIP Advances (August 2023)



Physics of Fluids

Special Topics Open
for Submissions

[Learn More](#)



Probabilistic flux limiters

Cite as: Phys. Fluids **37**, 046112 (2025); doi: [10.1063/5.0254069](https://doi.org/10.1063/5.0254069)

Submitted: 20 December 2024 · Accepted: 21 March 2025 ·

Published Online: 7 April 2025



View Online



Export Citation



CrossMark

Nga Nguyen-Fotiadis,¹  Robert Chiodi,²  Michael McKerns,¹  Daniel Livescu,²  and Andrew Sornborger^{1,a)} 

AFFILIATIONS

¹Information Sciences, CCS-3, Los Alamos National Laboratory, Los Alamos, New Mexico 87545, USA

²Computational Physics and Methods, CCS-2, Los Alamos National Laboratory, Los Alamos, New Mexico 87545, USA

^{a)} Author to whom correspondence should be addressed: sornborg@lanl.gov

ABSTRACT

The stable numerical integration of shocks in compressible flow simulations relies on the reduction or elimination of Gibbs phenomena (unstable, spurious oscillations). A popular method to virtually eliminate Gibbs oscillations caused by numerical discretization in under-resolved simulations is to use a flux limiter. A wide range of flux limiters have been studied in the literature, with recent interest in their optimization via machine learning methods trained on high-resolution datasets. The common use of flux limiters in numerical codes as plug-and-play blackbox components makes them key targets for design improvement. Even for deterministic dynamical models, numerical uncertainty is introduced via coarse-graining required by insufficient computational power to solve all scales of motion. Conventional flux limiters are deterministic and lack the capacity to address uncertainties, both aleatoric (inherent randomness) and epistemic (modeling uncertainty due to limited knowledge), which arise in coarse-grained numerical simulations. Here, we introduce a conceptually distinct type of flux limiter that is designed to handle the effects of randomness in the model and uncertainty in model parameters. Unlike traditional single-function flux limiters, these new *probabilistic flux limiters* incorporate multiple flux limiting functions, each applied with a learned probability drawn from high-resolution data to mitigate the effects of uncertainty in numerical simulations. This approach departs from traditional single-function limiters by explicitly modeling and incorporating uncertainty into the shock capturing process. Using the example of Burgers' equation as a testbed, we show that a machine learned, probabilistic flux limiter may be used in a shock capturing code to more accurately capture shock profiles. In particular, we show that our probabilistic flux limiter outperforms standard limiters and can be successively improved upon (up to a point) by expanding the set of probabilistically chosen flux limiting functions.

© 2025 Author(s). All article content, except where otherwise noted, is licensed under a Creative Commons Attribution (CC BY) license (<https://creativecommons.org/licenses/by/4.0/>). <https://doi.org/10.1063/5.0254069>

I. INTRODUCTION

Numerical methods for simulating fluid flows are inherently limited by the need to discretize the originally continuous flow equations. Since fully resolving all the dynamically relevant spatiotemporal scales is not feasible for most practical applications on today's computers, fluid dynamics computations are generally limited to the use of coarse meshes.

One of the most evident drawbacks of using coarse meshes arises when shocks form in compressible flows. This issue is significant in applications such as high-energy-density physics,¹ high-speed aerodynamics and hypersonic flight,² and supersonic combustion, detonation engines, or astrophysics, where accurate shock capture is critical. The physical width of the shock may be orders of magnitude smaller than the mesh spacing, which results in spurious oscillations in solution fluxes about the shock, unless an additional dissipation mechanism is provided to artificially widen the shock so it becomes representable on the actual mesh. This problem becomes more acute for higher order

schemes, which are desirable in smoother regions of the flow due to their lower truncation errors but which have less dissipation to regularize the coarse mesh equations around the shock. This type of oscillation due to the Gibbs effect³ does not occur for first-order flux approximations.

To resolve the tension between the benefit of using high-order derivatives when possible with the need to reduce the Gibbs effect, flux limiters were introduced in so-called shock capturing methods.^{4–8} A flux limiter, ϕ , interpolates between low- and high-order derivatives depending on the flux ratio between grid points in a numerical flow simulation, $r_i = \frac{u_i - u_{i-1}}{u_{i+1} - u_i}$, (here, u_i denotes a flow variable at grid location i). In regions of sharp differences between flow variables, first-order differences are favored in the interpolation to reduce spurious oscillations, but in smooth solution regions, high-order derivatives are favored to provide more accurate computation of flow quantities.

A wide range of flux limiters has been studied in the literature.⁹ Many of these limiters were designed to fit within the 2nd-order TVD

region.¹⁰ Full containment of a flux limiter within the 2nd-order TVD region is a sufficient, but not necessary, condition to eliminate the possibility of Gibbs effects in 2nd-order shock capturing schemes [see discussion around Eqs. (2.15) and (2.16) in Ref. 10] Some standard flux limiters, such as the van Albada limiter, work well but do not fit within this region. Similarly, machine learned flux limiters for the coarse-grained Burgers' equation have a unique functional appearance and lie outside the 2nd-order TVD region, yet still outperform other limiters in accuracy.¹¹ All limiters previously considered in the literature^{9,11} consist of a single flux limiting function, $\phi(r)$, used to deterministically interpolate between first- and high-order fluxes. None of the existing methods account for the randomness (e.g., parameter sensitivities¹² and subgrid variability¹³) in the problem.

This article is a first attempt to account for the probabilistic nature of the problem. Our primary contribution in this article is the introduction of a new, probabilistic conception of flux limiters.

In the presence of incomplete, imperfect knowledge (sometimes called epistemic uncertainty) about the operators involved in integrating non-linear flows, and especially in a high-consequence decision-making context, it makes sense to adopt a conservative posture to uncertainty quantification (UQ). This, in turn, naturally leads to UQ being posed as an optimization or machine learning problem, as this can facilitate estimates of bounds on the quantities of interest in the system, in our case a flux limiter.

Often, the UQ objective is to determine or estimate the expected value of some measurable quantity of interest, given an input distribution and a response function. However, in practice, the true response function and input distribution are rarely known precisely. Commonly, there may be some knowledge about the probability distribution and response function (perhaps through measurements performed with some degree of statistical confidence) such that the true input distribution and response function are bounded by knowledge of the system. This information can then be encapsulated in a probability measure—what a Bayesian probabilist would call a prior—so that we can perform (an optimization or) sampling to (calculate or) estimate (bounds on) the expected value of the quantity of interest by transforming the problem coordinates into a hypercube that includes the original coordinates X and the probability P associated with the position on X as defined by the probability measure.^{14,15}

With this in mind, here we consider coarse-grained flow simulations to be non-deterministic, since they necessarily ignore subgrid information. Below, we discuss a framework for implementing a type of shock capturing method that uses a (simple) probabilistic structure for a shock capturing scheme, where a fluid simulation is thought of as a probabilistic operator on data sampled from a distribution.

Specifically, we introduce a new type of flux limiter—a probabilistic flux limiter (see Fig. 1). We have taken the approach of using concepts from uncertainty quantification to learn optimal flux limiters in a Monte Carlo context. The resulting probabilistic flux limiter consists of a set of flux limiters with associated probabilities, $\{(\phi_m, p_m) : m \in [1, \dots, N_D]\}$, where $\sum_m^{N_D} p_m = 1$. In contrast to standard, deterministic flux limiters (Fig. 1, top panel), each evaluation of a probabilistic flux limiter (Fig. 1, bottom panel) randomly selects one of N_D limiters from a probability distribution to be used in the flux computation.

Below, with the example of Burgers' equation^{16–18} we demonstrate that probabilistic flux limiters may be learned for coarse-grained

fluid simulations from high-resolution data. We further show that they outperform other non-probabilistic flux limiters from the literature, including deterministic machine learned flux limiters. We use Burgers' equation as a benchmark problem due to its exact solvability, allowing precise evaluation of limiter performance. While our focus here is on flux limiters, our approach can be readily extended to slope limiters.

II. METHODS

To evaluate the performance of probabilistic flux limiters, we employ a numerical framework based on the 1D viscous Burgers' equation. This choice allows us to rigorously test shock-capturing performance under controlled conditions with an exactly solvable benchmark problem. The equation is discretized on a coarse grid, and we simulate shocks using a second-order shock capturing scheme with flux limiters. Our machine learning approach is designed to optimize the probabilistic flux limiter by minimizing discrepancies between coarse-grained simulations integrated with flux limiter scheme and high-resolution ground truth data. To facilitate handling the data, the coarse grid discretization is a subset of the points on the fine grid.

A detailed framework for our machine learned flux limiter theory was introduced in.¹¹ Below, we first summarize the deterministic, second-order shock capturing method that we used, show how we parameterized the flux limiter, and how we optimized the discretized limiter. We then go on to show how to modify this approach for a probabilistic flux limiter.

For low- and high resolution, respectively, we choose Lax-Friedrichs (LF)

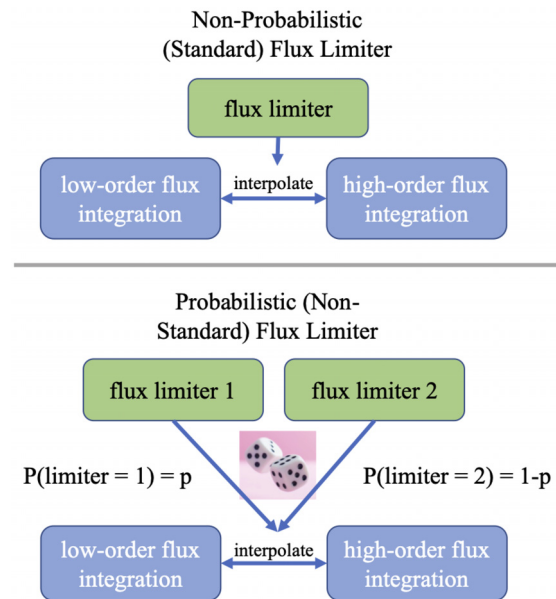


FIG. 1. A probabilistic flux limiter expands the flux limiter concept from an individual, deterministic interpolating function (top panel) to a set of interpolating functions applied probabilistically with probabilities drawn with replacement from a distribution learned from high-resolution data (bottom panel). In the example shown here, the probabilistic limiter consists of two flux limiters randomly selected with probability p and $1 - p$ for each flux computation.

$$f_{i\pm\frac{1}{2}}^{\text{low}} = f_{i\pm\frac{1}{2}}^{\text{LF}} = \frac{1}{2} \left[F(u_i) + F(u_{i+1}) \mp \alpha \frac{\Delta x}{\Delta t} (u_{i\pm 1} - u_i) \right], \quad (1)$$

$$\alpha = \max_u \left| \frac{\partial F}{\partial u} \right|,$$

and Lax–Wendroff (LW) fluxes

$$f_{i\pm\frac{1}{2}}^{\text{high}} = f_{i\pm\frac{1}{2}}^{\text{LW}}$$

$$= \frac{1}{2} \left[F(u_i) + F(u_{i+1}) \mp \frac{\Delta t}{\Delta x} \left(\frac{\partial F}{\partial u} (u_{i\pm\frac{1}{2}}) \right) (F(u_{i\pm 1}) - F(u_i)) \right], \quad (2)$$

where $F = \frac{u^2}{2} - \nu \frac{\partial u}{\partial x}$ is the flux defined for Burgers' equation. We now write the conservative form of Burgers' equation as

$$u_i(t_{n+1}) = u_i(t_n) - \frac{\Delta t}{\Delta x} \Delta F^i, \quad (3)$$

with

$$\Delta F^i = \Delta F_1^i + \phi(r_i) \Delta F_2^i + \phi(r_{i-1}) \Delta F_3^i, \quad (4)$$

where ΔF_1^i , ΔF_2^i , and ΔF_3^i are written explicitly as

$$\Delta F_1^i = f_{i+\frac{1}{2}}^{\text{LF}} - f_{i-\frac{1}{2}}^{\text{LF}},$$

$$\Delta F_2^i = f_{i+\frac{1}{2}}^{\text{LW}} - f_{i-\frac{1}{2}}^{\text{LW}}, \quad (5)$$

$$\Delta F_3^i = - \left(f_{i-\frac{1}{2}}^{\text{LW}} - f_{i-\frac{1}{2}}^{\text{LF}} \right).$$

We discretize the flux-limiter that we will optimize, $\phi(r)$, in piecewise linear segments, where the k th segment has the form

$$\phi_k(r) = \phi_0 + b_1(r_2 - r_1) + b_2(r_3 - r_2) + \dots + b_k(r - r_k) + 0_{k+1} + \dots + 0_K, \quad (6)$$

and $r \in [r_k, r_{k+1}]$, $k \in \{1, \dots, K\}$, $\phi_0 = 0$, and b_i are slope coefficients. Note that for $r \leq 0$, $\phi(r) = 0$ and for $r = r_K$, all terms in Eq. (6) are non-zero. Below, we use vector notation, $\mathbf{b} = [b_1, b_2, \dots, b_k, b_{k+1}, \dots, b_K]^T$ for slope coefficients. Equation (6) can be rewritten as $\phi_k(r) = \mathbf{b}^T \Delta \mathbf{r}_k$ with $\Delta \mathbf{r}_k$ defined as

$$\Delta \mathbf{r}_k = [r_2 - r_1, r_3 - r_2, \dots, r - r_k, 0, \dots, 0]^T. \quad (7)$$

To optimize the discretized flux-limiter in Eq. (6), we define the mean squared error between N input–output pairs, $\{o_i(\{u_c^i\}), g_i\}$

$$C = \frac{1}{2} \sum_{i=1}^N (o_i(\{u_c^i\}) - g_i)^2, \quad (8)$$

as the cost. Here, g_i is the high-resolution fluid velocity at the corresponding i th coarse grid position at time t_{n+1} , N is the number of coarse grid points, and o_i is the shock-capturing method's prediction of the fluid velocity at time t_{n+1} from data at the previous time step. o_i is a functional of a subset of data points $\{u_c^i\} = \{u_c^{i1}, u_c^{i2}, u_c^{i3}, \dots, u_c^{iN_c}\}$ indicated relative to the i th grid position at time step t_n . Here, we used $N_c = 6$ data points at time t_n to predict a data point g_i at t_{n+1} , i.e., $\{u_c^i\} = \{u_{i-3}, u_{i-2}, u_{i-1}, u_i, u_{i+1}, u_{i+2}\}$. Thus, $o_i(\{u_c^i\})$ is the integration obtained with the flux-limiter method defined in Eqs. (1), (2), (6) given a set of 6-points $\{u_c^i\}$

$$o_i(\{u_c^i\}, t_{n+1}) = u_i(t_n) - \frac{\Delta t}{\Delta x} \Delta F^i(\{u_c^i\}, \{b_i\}, t_n). \quad (9)$$

Here, $\Delta F^i(\{u_c^i\}, \{b_i\}, t_n)$, defined via Eqs. (4) and (5), is the difference of the two fluxes. The minimum of the cost function, Eq. (8), can be computed exactly by finding the unique root, \mathbf{b} , of the equation $\frac{\partial C}{\partial \mathbf{b}} = \mathbf{0}$, that is,

$$\sum_{i=1}^N \left(u_i - g_i - \frac{\Delta t}{\Delta x} \Delta F^i \right) \left(- \frac{\Delta t}{\Delta x} \right) \Delta \mathbf{s}_i \Delta F_{2,3}^i = \mathbf{0}. \quad (10)$$

In Eq. (10), $\Delta F^i = \Delta F(\{u_c^i\}, \{b_i\}, t_n)$ is defined via Eqs. (4) and (5). $\Delta \mathbf{s}_i = [\Delta \mathbf{r}_i, \Delta \mathbf{r}_{i-1}]$ is a $K \times 2$ matrix with $\Delta \mathbf{r}_i$ defined in Eq. (7). $\Delta F_{2,3}^i = [\Delta F_2^i, \Delta F_3^i]^T$ with components ΔF_2^i and ΔF_3^i defined via Eq. (5). Solving Eq. (10) reduces to solving a linear equation $\mathbf{A} \cdot \mathbf{b} = \mathbf{C}$ that yields $\mathbf{b} = \mathbf{A}^{-1} \cdot \mathbf{C}$. Here, $\mathbf{A} = \Delta \mathbf{r}_F \cdot (\Delta \mathbf{r}_F)^T$ and $\mathbf{C} = \frac{\Delta x}{\Delta t} \sum_{i=1}^N \times O_G^i \Delta \mathbf{r}_F^i$, where $\Delta \mathbf{r}_F$ is a $K \times N$ matrix with each column $\Delta \mathbf{r}_F^i$ a $K \times 1$ vector defined as $\Delta \mathbf{r}_F^i = (\Delta \mathbf{s}_i)(\Delta F_{2,3}^i)$. Finally, $O_G^i = u_i - g_i - \frac{\Delta t}{\Delta x} \Delta F_1^i$. Note that ΔF_1^i is defined via Eq. (5) and we recall that K is the size of the discretized flux limiter (i.e., the size of \mathbf{b}). Hence, each matrix \mathbf{A} (or \mathbf{C}) is a function of N training data points. We chose to discretize the flux limiter such that each segment contained an equal number of training data points.

In Ref. 11, we investigated the machine learning of deterministic flux limiters and found solutions obtained by optimizing with respect to a range of parameters, including coarse graining, the total degrees of freedom of the limiter, and the viscosity, (CG, K, μ) . This was essentially a meta-analysis given the costs, C (8), across the full parameter ranges. Below, we extend this machine learning approach to optimizing probabilistic flux limiters (see Fig. 2).

If we define our coordinate space, \mathcal{X} , by (CG, K, μ) , then transformation into measure space gives us $(\mathcal{X}, \mathcal{P})$, with \mathcal{P} defined by (P_{CG}, P_K, P_μ) . In this approach, our previous, deterministic flux limiters¹¹ were described by a probability distribution that was composed of a single Dirac delta function in each direction in measure space (and hence was deterministic). The number of Dirac delta functions used was $N_D = (1, 1, 1)$, or more compactly, $N_D = 1$.

In the current work, we extend our flux limiters to have a probabilistic nature by defining our probability measure to be composed of up to $N_D = 3$ Dirac delta functions per direction. As we will assume we have incomplete information on μ , but can specify CG and K exactly, we have $N_D = (1, 1, 3)$. From here onward, as we only have uncertainty in μ , we will use the compact form of N_D , and will denote \mathcal{P} simply with $p := P_\mu$ as a fourth coordinate. The resulting probabilistic flux limiter can then be thought of as a set of piecewise-linear flux limiters with associated selection probabilities, $\{(\phi_m, p_m) : m \in [1, \dots, N_D]\}$, with $\sum_{m=1}^{N_D} p_m = 1$. Each limiter $\phi_m := \phi_m(CG, K, \mu)$ can then be optimized on the coordinate hypercube defined by (CG, K, μ, p) .

For the probabilistic flux limiters, $\{(\phi_m, p_m) : m \in [1, \dots, N_D]\}$, that we consider here, with $N_D = 1, 2, 3$, we have

$$\Delta F \equiv \Delta F(\{u_c^i\}, \{b_i^m\}, \{p_m\}, \{\mu_m\}, t_n), \quad (11)$$

replacing ΔF in Eq. (9).

A. Dataset

High-resolution data were generated by solving Burgers' equation with a fine spatial resolution ($\Delta x = 2.5 \times 10^{-3}$ on a domain $x \in [-1, 1]$) and a small time step ($\Delta t = 10^{-4}$ for a time interval $t \in [0, 0.4]$). Random initial conditions with smooth profiles were

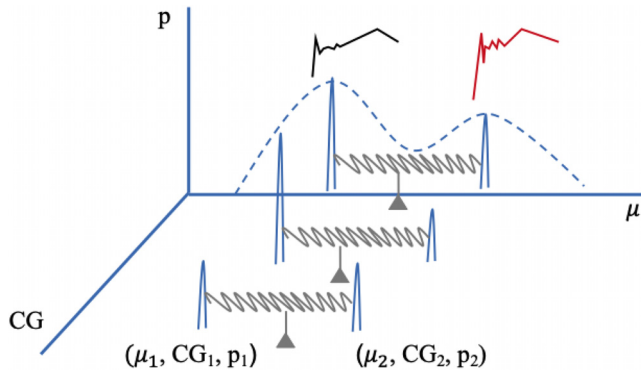


FIG. 2. Cartoon of the hypercube of inputs for the optimization of a probabilistic flux limiter. A mean constraint on viscosity (μ) is visualized as a fulcrum, and a variance constraint on μ is seen as a spring. Inputs to a flux limiter are specified by coarse graining (CG), total degrees of freedom of the limiter (K), and probability-weighted viscosity (μ, p). In this figure, the probability distribution of possible flux limiters is modeled by a discrete distribution of μ composed of $N_D = 2$ Dirac delta functions optimized over the parameter space (CG, K, μ, p) with $\sum_m^{N_D} p_m = 1$. In the text, we explore distributions of μ with up to $N_D = 3$.

used to ensure a diverse set of solutions, including steep gradients and shocks. The dataset consists of 60 distinct Burger’s high-resolution simulations evolved from 60 random initial conditions. Among these 60 simulations, 50 simulations (80%) were allocated for training and

the remaining ten simulations (20%) reserved for testing. For each simulation, coarse-grained data were derived by subsampling the HR data using a coarse-graining within the range $CG = [2, 3, \dots, 10]$ to represent different levels of resolution. For each CG simulation, the total number of training data points that enter the cost function is thus 160M divided by the corresponding CG factor. During training, the cost function decreased to small values, indicating good convergence.

B. Probabilistic solutions

Figure 3 captures the results of an optimization of a probabilistic flux limiter over a parameter space with $CG = [2, 3, \dots, 10]$, $K = [2, 3, \dots, 38]$, and $\mu = [0.002, 0.03]$ with probabilities $p_i = [0, 1]$ with the constraint $p = p_1 + p_2 + p_3 = 1$ and $N_D = 3$. Mean and variance constraints defining the range of viscosities μ_m were tuned to be, respectively, $4.0e^{-3}$ and $1.0e^{-4}$. Typically, stable solutions were attained [see Fig. 3(a)–3(c)] after approximately 60 iterations of the optimizer.

The three blue curves in Fig. 3(a) main plot and inset represent the three corresponding pairs (μ_i, p_i) , where we use the same line style for each pair. The dominant contributions to the optimized limiters came from (μ_1, p_1) and (μ_2, p_2) while the remaining pair (μ_3, p_3) contributed at a lower probability to the solution.

Explicit values for the endpoints of the linear segments and the slopes of the piecewise-linear flux limiting functions are presented in Tables VII and VIII in the Appendix. The optimization for the limiter

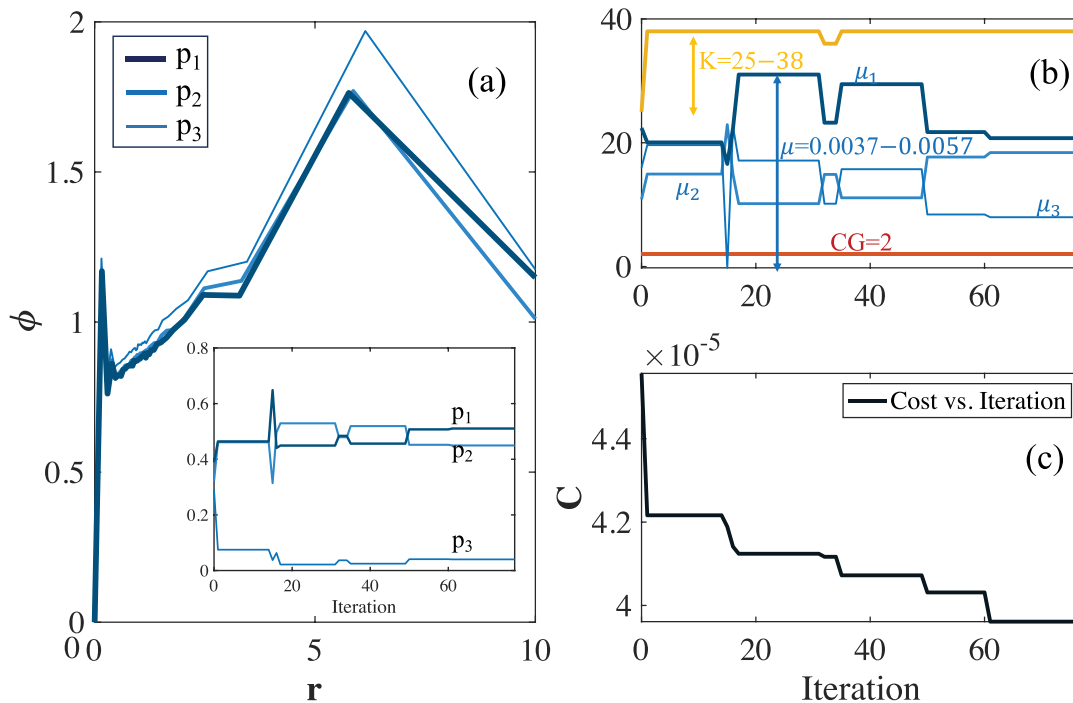


FIG. 3. Optimization of a probabilistic flux limiter with $N_D = 3$. (a) Optimized forms of the three flux limiting functions ϕ_1, ϕ_2 , and ϕ_3 after 60 iterations, the thicker the line the larger the probability. The probability distribution of the three corresponding viscosity values, μ_1, μ_2 , and μ_3 [also shown in (b)] as a function of training iteration are depicted in the inset. (b) Plot of the three viscosity values μ_1, μ_2 , and μ_3 , bin number K , and coarse graining CG vs iteration step. (c) Value of the cost function vs iteration step. Optimization was performed on the entire parameter space $CG = [1, 2, \dots, 10]$, $K = [2, 3, \dots, 38]$, $\mu = [0.002, 0.03]$ with $p = p_1 + p_2 + p_3 = 1$.

20 April 2025 03:11:49

TABLE I. Mean reconstruction errors (e_{mean}) obtained on the test set (data not trained and random initial conditions) using machine learned probabilistic flux limiters ($N_D = 1, 2, 3$) as compared to van Leer and van Albada 2. Learned flux limiters were optimized on the entire parameter range of $K = [2, 3, \dots, 38]$, $CG = [2, 3, \dots, 10]$, and all μ_i 's are constrained to be in the interval $\mu_i = [0.002, 0.03]$.

FLs	van Leer	van Albada 2	$N_D = 1$	$N_D = 2$	$N_D = 3$
Mean Error	0.71×10^{-3}	0.0768×10^{-3}	0.0762×10^{-3}	0.0758×10^{-3}	0.0753×10^{-3}

TABLE II. Mean reconstruction errors (e_{mean}) obtained on the test set (data not trained and random initial conditions) using machine learned probabilistic flux limiters ($N_D = 1, 2, 3$) as compared to van Leer and van Albada 2 for $CG = 8$. Learned flux limiters were optimized while constraining the coarse graining to $CG = 8$ and the other parameters are in the ranges $K = [2, 3, \dots, 38]$, and $\mu_i = [0.002, 0.03]$.

FLs	van Leer	van Albada 2	$N_D = 1$	$N_D = 2$	$N_D = 3$
Mean Error	0.71×10^{-3}	0.0768×10^{-3}	0.0764×10^{-3}	0.0761×10^{-3}	0.0754×10^{-3}

in Fig. 3 was performed over the entire computational parameter range, giving a limiter that worked best on average in this parameter space. An additional probabilistic flux limiter is depicted in the Appendix, Fig. 5. For the optimization in Fig. 5, the coarse graining parameter was constrained to $CG = 8$. Note the differences found toward the tail (large r) of the flux limiters in Figs. 3 and 5, resulting from the tighter constraint on CG .

We studied probabilistic flux limiters obtained for the cases $N_D \in [1, 2, 3]$ (i.e., sets of one, two, or three flux limiting functions with associated selection probabilities) and compared these probabilistic flux limiters with van Leer and van Albada 2 (note that the $N_D = 1$ case was studied in Ref. 11 and was shown to outperform 12 flux limiters, including van Leer and van Albada 2, from the literature. In Tables I and II, we present mean squared errors (MSEs) measuring the shock capturing prediction $\{o_i\}$ as compared to ground truth, high-resolution data $\{g_i\}$

$$e_{\text{mean}} = \frac{1}{2N} \sum_{i=1}^N (o_i - g_i)^2. \tag{12}$$

In Tables III and IV, we present MSE between a sinusoidal solution to Burgers' equation and the shock capturing prediction. For $N_D = 1$, our learned limiter performs as well or better than the deterministic van Leer and van Albada 2 limiters across a wide range of coarse-graining factors ($CG = 2$ to 10).¹¹ For $N_D = 2$, the learned probabilistic limiter shows a marked improvement in shock representation for smaller viscosities ($\mu \in [0.002, 0.01]$) where sharper gradients are more prevalent. For $N_D = 3$, the learned limiter achieves the highest accuracy across the full range of tested viscosities ($\mu \in [0.002, 0.03]$), with diminishing returns compared to $N_D = 2$. This diminishing gain suggests that two dominant limiters are often sufficient for accurate reconstructions.

TABLE III. Mean reconstruction errors (e_{mean}) obtained with sinusoidal initial condition using machine learned probabilistic flux limiters ($N_D = 1, 2, 3$) as compared to van Leer and van Albada 2. Learned flux limiters were optimized on the entire parameter range of $K = [2, 3, \dots, 38]$, $CG = [2, 3, \dots, 10]$, and all μ_i 's are constrained to be in the interval $\mu_i = [0.002, 0.03]$.

FLs	van Leer	van Albada 2	$N_D = 1$	$N_D = 2$	$N_D = 3$
Mean Error	0.926×10^{-3}	0.235×10^{-3}	0.367×10^{-3}	0.194×10^{-3}	0.189×10^{-3}

For $N_D > 1$, we obtain at least two pronounced contributions to the total probability distribution. For $N_D = 2$, our optimization yielded two Dirac delta functions with strong (i.e., high probability) contributions of $p_i \approx 0.5$ each, while for $N_D = 3$ our optimization is shown in Fig. 3 with two flux limiters with strong contributions and one flux limiter with stable but smaller probability, $p_3 \approx 0$.

In Table V, we evaluated MSE obtained from five characteristic viscosities, μ (left column), on test cases with sinusoidal initial conditions, using machine-learned probabilistic flux limiters (for $N_D = 1, 2, 3$). These errors are compared to traditional van Leer and van Albada 2 methods, with a coarse graining of $CG = 8$. The optimization of learned flux limiters was thus constrained by $CG = 8$, with other parameters varying within $K = [2, 3, \dots, 38]$ and $\mu_i = [0.002, 0.03]$. We used $CG = 8$, corresponding to $dt = 8 \times 1.0e^{-4}$ and $dx = 8 \times 2.5e^{-3}$. The lower bound case of $\mu = 0.002$ is depicted in the top row. The viscosity ($\mu = 0.00498$) was average of the three associated viscosities obtained with the $N_D = 3$ flux limiter. This was also the case with $N_D = 2$ flux limiters. The next viscosity ($\mu = 0.00625$) was derived from $N_D = 1$ flux limiter, and the final two μ values were selected from the lower and upper bounds of the viscosities used over which we trained the probabilistic flux limiter. Details of the probabilistic flux limiters' optimized characteristic parameters are shown in Table VI.

In Fig. 4, we plot solutions to the analytically solvable sine wave problem obtained using probabilistic flux limiters for $N_D \in [1, 2, 3]$ in comparison with ground truth (blue connected circles), van Leer, and van Albada 2 for $\mu = 0.002$. Note that this plot captures a sufficiently large time such that the shock has evolved to be sharp. All machine learned probabilistic flux limiters outperformed van Leer and van Albada 2 limiters, with the $N_D = 3$ case (black dashed line) performing with the highest accuracy. This result was consistent across all

TABLE IV. Mean reconstruction errors (e_{mean}) obtained with sinusoidal initial condition using machine learned probabilistic flux limiters ($N_D = 1, 2, 3$) as compared to van Leer and van Albada 2 for $CG = 8$. Learned flux limiters were optimized while constraining the coarse graining to $CG = 8$ and the other parameters are in the ranges $K = [2, 3, \dots, 38]$, and $\mu_i = [0.002, 0.03]$.

FLs	van Leer	van Albada 2	$N_D = 1$	$N_D = 2$	$N_D = 3$
Mean Error	0.926×10^{-3}	0.235×10^{-3}	0.063×10^{-3}	0.031×10^{-3}	0.024×10^{-3}

TABLE V. MSE [Eq. (12)] comparing high-resolution and flux limiter-based simulations averaged over $t = [0, 0.4]$ and $x = [-1, 1]$ for five different μ with sinusoidal initial conditions. Here, we compare machine learned probabilistic flux limiters ($N_D = 1, 2, 3$) to van Leer and van Albada 2 for a coarse-graining $CG = 8$. The learned probabilistic flux limiter was optimized over the ranges $K \in [2, 3, \dots, 38]$ and $\mu_i \in [0.002, 0.03]$. The left column represents viscosities of a set of high-resolution (ground truth) simulations taken from the range of viscosities that the probabilistic flux limiter was trained on. Numbers in bold show the superior performance. Note that all of the best performance results were for machine learned limiters. For small viscosities (upper three rows), probabilistic flux limiters with $N_D = 3$ were best able to capture the sharper shocks.

μ	van Leer	van Albada 2	$N_D = 1$	$N_D = 2$	$N_D = 3$
0.002	2.33×10^{-3}	0.60×10^{-3}	0.62×10^{-3}	0.46×10^{-3}	0.42×10^{-3}
0.004 98	2.08×10^{-3}	0.46×10^{-3}	0.41×10^{-3}	0.27×10^{-3}	0.24×10^{-3}
0.006 25	1.89×10^{-3}	0.44×10^{-3}	0.37×10^{-3}	0.20×10^{-3}	0.17×10^{-3}
0.02	1.02×10^{-3}	0.23×10^{-3}	0.001×10^{-3}	0.03×10^{-3}	0.046×10^{-3}
0.03	0.73×10^{-3}	0.16×10^{-3}	0.11×10^{-3}	0.25×10^{-3}	0.29×10^{-3}

considered values of μ , spanning the entire range from lower bound to upper bound, as detailed in Table V.

It is important to note that when $N_D = 1$, the learned limiter performed very well for the larger viscosity band but had a marginally lower performance compared to van Albada 2 across the entire time interval $[0, 0.4]$ at small viscosities. Specifically when $\mu = 0.002$, van Albada 2 provided a slightly better solution than $N_D = 1$ at early times before shocks occurred. For $N_D = 1, 2, 3$, the same optimized solutions were employed across all study cases. In contrast, distinct solutions utilizing van Leer and van Albada 2, along with corresponding ground truths, were derived for each μ . Thus, we expect that there should be one viscosity for which the $N_D = 1$ limiter should match very well the ground truth data. On the other hand, the $N_D > 1$ limiters exhibit smaller overall errors over the whole range of viscosities and greater generalizability potential when the viscosity is scaled by the ground truth viscosity (see below).

For sinusoidal initial conditions, the learned probabilistic flux limiters provided accurate shock reconstructions, maintaining stability across the full range of tested viscosities. Furthermore, by scaling the effective viscosities (μ_m) of the learned probabilistic flux limiters to match test cases, the probabilistic framework retained accuracy even outside its original training domain. This demonstrates the generalizability of probabilistic flux limiters to untrained cases.

TABLE VI. Optimal selection probabilities, p_i , and associated viscosities, μ_i , of probabilistic flux limiter functions used in Table V.

$N_D = 1$		$N_D = 2$		$N_D = 3$	
p	μ_1	p	μ_{1-2}	p	μ_{1-3}
1	0.006 25	0.09	0.005 62	0.09	0.005 11
		0.91	0.004 92	0.08	0.004 39
				0.83	0.005 02

To assess the practical feasibility of probabilistic flux limiters, we compared their computational cost and memory footprint against standard deterministic limiters. While probabilistic flux limiters introduce an additional step of probabilistic selection, our implementation maintains a comparable computational cost to standard flux limiters, with only a marginal increase in overhead ($\sim 5\% - 7\%$) due to the storage of learned probability distributions. Importantly, the accuracy improvements gained by using probabilistic flux limiters justify this minor computational tradeoff, particularly in under-resolved regimes where traditional methods struggle.

C. Robustness and generalizability

In Table V, we studied a fixed probabilistic flux limiter learned across various viscosities μ . In the Appendix, Table IX, we show that, by scaling the μ_i values associated with a probabilistic flux limiter with the μ value of the high-resolution simulation, we can further extend the domain of application of the limiter. This demonstrates the benefit of viscosity scaling outside the optimal range expected from our machine learning procedure.

The $N_D = 3$ case consistently showed the best performance: mean profile indicating a sharper shock than the deterministic limiters with smaller standard deviation, demonstrating its effectiveness in handling coarse-grained simulations. Even though we plotted standard deviation bands taken from 100 test runs, the widths of the bands were barely distinguishable from the unaveraged lines plotted for the non-probabilistic flux limiters.

The $N_D = 3$ case, in both Tables V and IX, slightly outperformed the $N_D = 2$ case, while the traditional flux limiters of van Leer or van Albada 2, i) had lower accuracy than that produced with machine learned probabilistic flux limiters, and ii) showed “kinks” in the shock reconstructions as compared to the smooth shock reconstructions obtained by our probabilistic limiters. These kinks occurred when μ was sufficiently small. For instance, van Albada 2 exhibited oscillations for $\mu = 0.002$, whereas the oscillations disappeared at higher

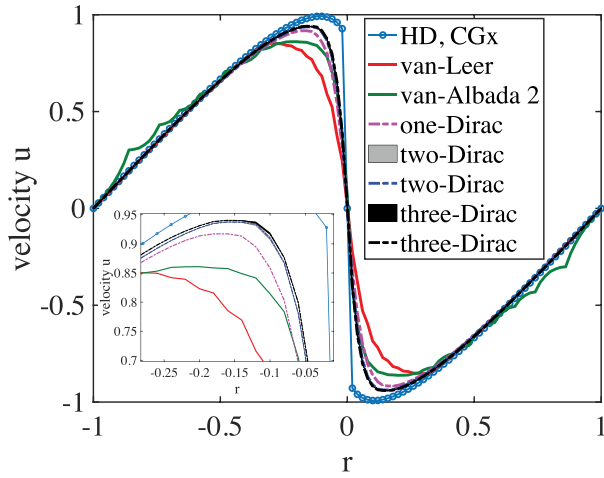


FIG. 4. Shock reconstruction in the case of Burgers' equation learned with $N_D \in [1, 2, 3]$ Dirac delta functions as compared to van Leer and van Albada 2 cases. Ground truth is plotted as blue connected circles (HD). The inset is a magnification of the solution at the upper left of the shock. Note that the probabilistic flux limiters in this figure are plotted as gray ($N_D = 2$) and black ($N_D = 3$) bands indicating mean plus and minus standard deviation. The probabilistic flux limiter with $N_D = 3$ used in this plot is given in Tables VII and VIII.

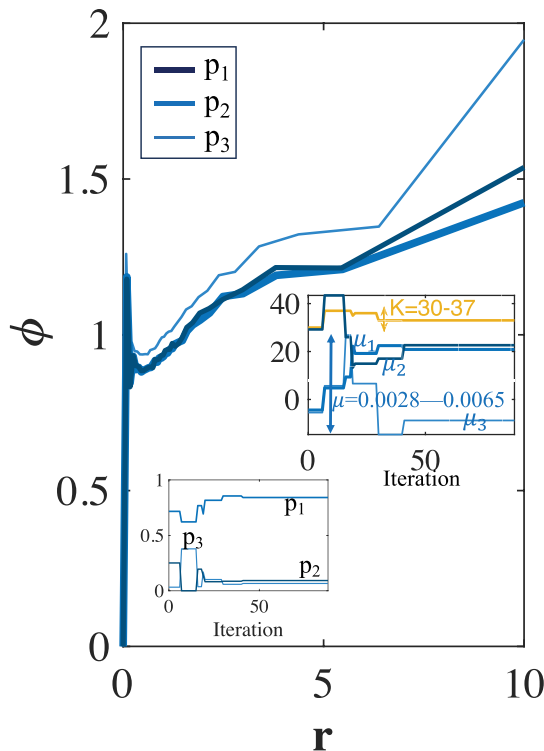


FIG. 5. Probabilistic flux limiter with coarse graining constraint. A probabilistic flux limiter obtained with $N_D = 3$ and constraint $CG = 8$. Top inset is parameter convergence with respect to optimization iteration and bottom inset is probability p_1, p_2, p_3 corresponding to the weights of the three Dirac delta functions as a function of optimization iteration.

viscosities (e.g., $\mu = 0.1$). As a control run, we examined van Albada 2 solutions with larger μ values (e.g., $\mu = 0.1$, larger viscosity) and these “oscillations” disappeared. In contrast, probabilistic flux limiters maintained smooth, monotonic profiles across all tested viscosity ranges, demonstrating their robustness even under challenging conditions.

The improvement in performance going from $N_D = 2$ to $N_D = 3$ was significantly less than the improvement going from $N_D = 1$ to $N_D = 2$. This (and consistently obtaining $p_3 \geq 0$) suggests that the $N_D = 3$ Dirac delta function case well approximates a distribution that is sufficient to produce an optimal probabilistic limiter for the system under consideration. While higher-order cases ($N_D > 3$) could theoretically be explored, the current results suggest that $N_D = 3$ effectively balances accuracy and training cost for the studied problem. By leveraging their probabilistic structure, probabilistic flux limiters are not only robust to variations in input conditions but also adaptable to new scenarios. While static shocks serve as a rigorous benchmark due to their exact solvability, our probabilistic flux limiter framework is not restricted to this situation. We have validated the applicability of our trained flux limiter to moving shocks, demonstrating steady reconstruction errors of $\approx 1.87 \times 10^{-5}$.

III. DISCUSSION

In this paper, we presented a conceptually new type of flux limiter that we refer to as a *probabilistic flux limiter* since its use consists of drawing randomly from a set of flux limiting functions, $\phi_m := \phi_m(CG, K, \mu)$, optimized on the parameter hypercube defined by (CG, K, μ, p) . Unlike deterministic flux limiters, probabilistic flux limiters leverage probabilistic selection to dynamically adapt to varying flow conditions, providing a robust framework for uncertainty quantification in coarse-grained simulations.

We quantified the effectiveness of machine learned probabilistic flux limiters for integrating a coarse-grained, one-dimensional Burgers' equation in time. High-resolution training data with diverse initial conditions allowed us to optimize probabilistic flux limiters for a wide range of flows. Probabilistic flux limiters were trained on coarse-grained data taken from a high-resolution dataset with random initial conditions. With the learned probabilistic flux limiter, we then integrated on unseen cases of both random and sinusoidal initial conditions.

Our results consistently showed that the learned probabilistic flux limiters can more accurately capture the overall coarse-grained evolution of the flow, and, in particular, shock formation relative to conventional flux limiters, e.g., van Leer and van Albada 2. We chose only these two common limiters from the literature for comparison since in our previous machine learning application of flux limiters to numerical solutions of the Burger's equation, they proved the most accurate compared to ten other flux limiters.¹¹

Note that in Fig. 3(b), the optimal coarse-graining over all possible coarse-grainings was 2 for this case. This should be considered as distinct from fixing $CG = 2$ and optimizing over other parameters. Further, the optimal K , in this case, was at the upper bound of the parameter space. By extending the parameter space, we could potentially have found better performance, but most of the segments in the limiter were found in the range $r \approx 1$, and it was likely that they would only marginally improve the limiter that was found.

The improvement that one finds as N_D is incremented decreases. This demonstrates that although there was significant improvement, there were also diminishing returns as N_D was increased from 2 to 3.

TABLE VII. Coordinates of three flux limiters in the case $N_D = 3$. Results obtained over the entire search range of $CG = [2, 3, \dots, 10]$, $K = [2, 3, \dots, 38]$, and μ_i 's are constrained to be in the interval $\mu_i = [0.002, 0.03]$.

	r_1	r_2	r_3	r_4	r_5	r_6	r_7	r_8	r_9	r_{10}	r_{11}	r_{12}	r_{13}	r_{14}	r_{15}	r_{16}	r_{17}	r_{18}	r_{19}	r_{20}	r_{21}	r_{22}
	r_{23}	r_{24}	r_{25}	r_{26}	r_{27}	r_{28}	r_{29}	r_{30}	r_{31}	r_{32}	r_{33}	r_{34}	r_{35}	r_{36}	r_{37}	r_{38}	r_{39}					
65	0.0	0.23	0.38	0.49	0.57	0.64	0.69	0.73	0.77	0.80	0.83	0.86	0.88	0.90	0.92	0.94	0.96	0.97	0.99	1.00	1.01	1.05
	1.07	1.09	1.11	1.13	1.16	1.13	1.19	1.22	1.27	1.33	1.41	1.52	1.69	1.96	2.51	4.15	10.00					
65	0.0	0.24	0.40	0.51	0.59	0.65	0.70	0.74	0.78	0.81	0.84	0.86	0.89	0.91	0.93	0.94	0.96	0.98	0.99	1.00	1.02	1.04
	1.05	1.07	1.09	1.11	1.13	1.15	1.18	1.22	1.26	1.32	1.40	1.50	1.66	1.92	2.45	4.03	10.00					
65	0.0	0.24	0.40	0.51	0.59	0.65	0.70	0.74	0.78	0.81	0.83	0.86	0.89	0.91	0.93	0.94	0.96	0.98	0.99	1.00	1.02	1.03
	1.05	1.06	1.08	1.10	1.12	1.15	1.18	1.21	1.26	1.31	1.39	1.49	1.65	1.91	2.42	3.98	10.00					

TABLE VIII. Slopes of flux limiters in the case $N_D = 3$. Results obtained over the entire search range of $CG = [2, 3, \dots, 10]$, $K = [2, 3, \dots, 38]$, and $\mu_i = [0.002, 0.03]$. p_i 's are in the interval $p_i = [0, 1]$ obeying unit sum for probability.

	b_1	b_2	b_3	b_4	b_5	b_6	b_7	b_8	b_9	b_{10}	b_{11}	b_{12}	b_{13}	b_{14}	b_{15}	b_{16}	b_{17}	b_{18}	b_{19}	b_{20}	b_{21}
	b_{22}	b_{23}	b_{24}	b_{25}	b_{26}	b_{27}	b_{28}	b_{29}	b_{30}	b_{31}	b_{32}	b_{33}	b_{34}	b_{35}	b_{36}	b_{37}	b_{38}				
65	5.14	-3.01	1.11	-0.46	0.27	0.28	0.16	0.15	-0.06	0.25	0.26	-0.27	0.39	-0.19	0.15	0.42	0.10	-0.22	0.46	-0.11	0.15
	0.07	0.24	-0.46	0.58	-0.25	0.41	0.01	0.02	0.19	0.02	0.18	0.12	0.01	0.27	0.24	0.34	-0.14				
65	4.93	-2.88	1.04	-0.45	0.55	-0.05	0.20	0.07	0.38	-0.38	0.31	0.61	-0.47	0.05	0.45	0.20	-0.29	0.09	-0.05	0.10	0.60
	-0.60	0.56	-0.04	-0.28	0.80	-0.61	0.43	0.26	-0.03	0.09	0.30	0.03	0.10	0.22	0.04	0.32	-0.15				
65	4.86	-2.90	1.24	-0.55	0.47	-0.08	0.13	0.17	-0.08	0.42	0.39	0.19	-0.46	0.53	0.05	0.10	-0.07	0.15	-0.01	0.31	0.07
	0.02	0.05	0.33	-0.20	0.16	-0.32	0.36	0.01	0.10	0.19	0.03	0.20	0.08	0.30	-0.05	0.32	-0.14				

We learned probabilistic flux limiters for N_D up to 3, which seemed to provide a sufficient number of Dirac delta functions to approximate the optimal probabilistic flux limiter for the system studied in this manuscript. The results obtained in this paper suggest potential applications of probabilistic flux limiters for better shock capture in more complex flow simulations. Flux limiters are widely used in computational fluid dynamics solvers for applications that involve shock waves, such as high-speed aerodynamics, supersonic combustion in ramjets, and defense applications. Our probabilistic flux limiter extends these methods by incorporating uncertainty, which accounts for subgrid phenomena in under-resolved simulations. As simulations in hypersonic flight, high-energy-density physics, and multi-material shock interactions grow in complexity, our method provides a robust framework for improving shock resolution and stability. While probabilistic

flux limiters offer significant advantages, certain tradeoffs remain. Scaling to high-dimensional problems and optimizing for real-time applications are active research areas. Additionally, while our results demonstrate robust performance across viscosity regimes, further validation on multi-material shock interactions is needed. These challenges are being addressed in our ongoing work extending probabilistic flux limiters to Euler and Navier–Stokes simulations in higher dimensions.

ACKNOWLEDGMENTS

Research presented in this article was supported by the NNSA Advanced Simulation and Computing Beyond Moore’s Law Program at Los Alamos National Laboratory and by the Uncertainty Quantification Foundation under the Statistical

TABLE IX. MSE obtained for five different viscosities μ , similar values as shown in Table V, on the test case of a sinusoidal initial condition using machine learned probabilistic flux limiters ($N_D = 1, 2, 3$) as compared to van Leer and van Albada 2 for $CG = 8$. Optimal flux limiters were learned while constraining the coarse graining to $CG = 8$ and the other parameters are in the ranges $K = [2, 3, \dots, 38]$, and $\mu_i = [0.002, 0.03]$. Unlike the results shown in Table V for $N_D = 1, 2, 3$ Dirac delta functions (where the learned flux limiters were trained at different μ than they were applied), here, these MSE were obtained with the limiter trained for the μ in the far left column. Bold numbers indicate superior performance.

μ	van Leer	van Albada 2	$N_D = 1$	$N_D = 2$	$N_D = 3$
0.002	2.33×10^{-3}	0.60×10^{-3}	0.49×10^{-3}	0.32×10^{-3}	0.29×10^{-3}
0.004 98	2.08×10^{-3}	0.46×10^{-3}	0.41×10^{-3}	0.27×10^{-3}	0.24×10^{-3}
0.006 25	1.89×10^{-3}	0.44×10^{-3}	0.037×10^{-3}	0.024×10^{-3}	0.021×10^{-3}
0.02	1.02×10^{-3}	0.23×10^{-3}	0.19×10^{-3}	0.11×10^{-3}	0.08×10^{-3}
0.03	0.73×10^{-3}	0.16×10^{-3}	0.14×10^{-3}	0.08×10^{-3}	0.06×10^{-3}

20 April 2025 03:11:49

Learning program. Los Alamos National Laboratory is operated by Triad National Security, LLC, for the National Nuclear Security Administration of the U.S. Department of Energy (Contract No. 89233218CNA000001). The Uncertainty Quantification Foundation is a nonprofit dedicated to the advancement of predictive science through research, education, and the development and dissemination of advanced technologies. This document's LANL designation is LA-UR-24-22187.

AUTHOR DECLARATIONS

Conflict of Interest

The authors have no conflicts to disclose.

Author Contributions

Nga Nguyen-Fotiadis: Conceptualization (equal); Data curation (equal); Formal analysis (equal); Investigation (equal); Methodology (equal); Resources (equal); Software (equal); Validation (equal); Visualization (equal); Writing – original draft (equal); Writing – review & editing (equal). **Robert Chiodi:** Conceptualization (equal); Data curation (equal); Formal analysis (equal); Investigation (equal); Methodology (equal); Resources (equal); Software (equal); Validation (equal); Visualization (equal); Writing – original draft (equal); Writing – review & editing (equal). **Michael McKerns:** Conceptualization (equal); Data curation (equal); Formal analysis (equal); Investigation (equal); Methodology (equal); Resources (equal); Software (equal); Validation (equal); Supervision (equal); Validation (equal); Visualization (equal); Writing – original draft (equal); Writing – review & editing (equal). **Daniel Livescu:** Conceptualization (equal); Data curation (equal); Formal analysis (equal); Investigation (equal); Methodology (equal); Resources (equal); Software (equal); Supervision (equal); Validation (equal); Visualization (equal); Writing – original draft (equal); Writing – review & editing (equal). **Andrew Sornborger:** Conceptualization (equal); Data curation (equal); Formal analysis (equal); Funding acquisition (equal); Investigation (equal); Methodology (equal); Project administration (equal); Resources (equal); Software (equal); Supervision (equal); Validation (equal); Visualization (equal); Writing – original draft (equal); Writing – review & editing (equal).

DATA AVAILABILITY

The data that support the findings of this study are available within the article and from the corresponding author upon reasonable request.

APPENDIX: PARAMETERS OF OPTIMIZED FLUX LIMITERS

Closed forms of the flux limiting functions (iteration 65) for $N_D = 3$ are found in [Tables VII](#) and [VIII](#).

We show in [Fig. 5](#) the flux limiting functions and probabilities (lower inset) at the termination of the optimization procedure for $N_D = 3$ with the constraint $CG = 8$. The yellow curve in the upper inset of [Fig. 5](#) represents the change in bin number K along with corresponding viscosity μ_1, μ_2, μ_3 and probability p_1, p_2, p_3 , respectively, in thick, medium, and thin solid lines (both insets).

The errors compared against several high-resolution simulations with different viscosities are shown in [Table IX](#). In this case, the training was performed with the same viscosity as the high-resolution case. For this application, increasing the number of Dirac delta functions in the description of the ML limiter always leads to lower errors.

REFERENCES

- R. P. Drake, *High-Energy-Density Physics: Fundamentals, Inertial Fusion, and Experimental Astrophysics* (Springer-Verlag, 2006).
- R. J. LeVeque, *Finite Volume Methods for Hyperbolic Problems* (Cambridge University Press, 2002).
- H. Wilbraham, "On a certain periodic function," *Cambridge Dublin Math. J.* **3**, 198–201 (1848).
- S. K. Godunov, "A difference scheme for numerical computation of discontinuous solutions of fluid dynamics," *Mat. Sb.* **47**, 271–306 (1959).
- B. Van Leer, "Towards the ultimate conservative difference scheme. v. a second-order sequel to Godunov's method," *J. Comput. Phys.* **32**(1), 101–136 (1979).
- P. Colella and P. R. Woodward, "The piecewise parabolic method (PPM) for gas-dynamical simulations," *J. Comput. Phys.* **54**(1), 174–201 (1984).
- A. Harten, "High resolution schemes for hyperbolic conservation laws," *J. Comput. Phys.* **135**(2), 260–278 (1997).
- C.-W. Shu and S. Osher, "Efficient implementation of essentially non-oscillatory shock capturing schemes," *J. Comput. Phys.* **77**(2), 439–471 (1988).
- D. Zhang, C. Jiang, D. Liang, and L. Cheng, "A review on TVD schemes and a refined flux-limiter for steady-state calculations," *J. Comput. Phys.* **302**, 114–154 (2015).
- P. K. Sweby, "High resolution schemes using flux limiters for hyperbolic conservation laws," *SIAM J. Numer. Anal.* **21**(5), 995–1011 (1984).
- N. T. T. Nguyen-Fotiadis, M. McKerns, and A. Sornborger, "Machine learning changes the rules for flux limiters," *Phys. Fluids* **34**, 1–11 (2022).
- W. L. Oberkampf and C. J. Roy, *Verification and Validation in Scientific Computing* (Cambridge University Press, 2010).
- S. B. Pope, "Ten questions concerning the large-eddy simulation of turbulent flows," *New J. Phys.* **6**, 35 (2004).
- H. Owahdi, C. Scovel, T. J. Sullivan, M. McKerns, and M. Ortiz, "Optimal uncertainty quantification," *SIAM Rev.* **55**(2), 271–345 (2013).
- See <http://arxiv.org/pdf/1202.1055v1> for M. McKerns, H. Owahdi, C. Scovel, T. J. Sullivan, and M. Ortiz, "The optimal uncertainty algorithm in the mystic framework," Caltech CACR Technical Report, August 2010.
- J. M. Burgers, "A mathematical model illustrating the theory of turbulence," in *Advances in Applied Mechanics* (Elsevier, 1948), Vol. 1, pp. 171–199.
- H. Eberhard, "The partial differential equation $u_t + u_x = \mu u_{xx}$," *Commun. Pure Appl. Math.* **3**(3), 201–230 (1942).
- J. D. Cole, "On a quasi-linear parabolic equation occurring in aerodynamics," *Q. Appl. Math.* **9**(3), 225–236 (1951).